Materials Science and Engineering B 264 (2021) 114913

Contents lists available at ScienceDirect

Materials Science & Engineering B

journal homepage: www.elsevier.com/locate/mseb

Photocatalytic and antifouling properties of electrospun TiO_2 polyacrylonitrile composite nanofibers under visible light

Chris Ademola Bode-Aluko [a,*], Omoniyi Pereao [a], Htet H. Kyaw [b], Laila Al-Naamani [c,d], Mohammed Z. Al-Abri [b], Myo Tay Zar Myint [e], Arnoux Rossouw [f,g], Olanrewaju Fatoba [a], Leslie Petrik [a], Sergey Dobretsov [c,d,*]

[a] Environmental and Nano Sciences Group, Department of Chemistry, University of the Western Cape, Bellville 7535, South Africa
[b] Nanotechnology Research Center, Sultan Qaboos University, 123 Al-Khoud, Muscat, Oman
[c] Department of Marine Science and Fisheries, Sultan Qaboos University, 123 Al-Khoud, PO Box 34, Muscat, Oman
[d] Center of Excellence in Marine Biotechnology, Sultan Qaboos University, 123 Al-Khoud, PO Box 50, Muscat, Oman
[e] Department of Physics, College of Science, Sultan Qaboos University, 123 Al-Khoud, Muscat, Oman
[f] Flerov Laboratory of Nuclear Reactions, Joint Institute for Nuclear Research, Dubna, Russia
[g] Department of Electrical and Electronic Engineering, Stellenbosch University, Stellenbosch 7600, South Africa

ARTICLE INFO

Keywords:
Photocatalysis
Antifouling
Nanofibers
Titanium (IV) oxide
Visible light

ABSTRACT

Polyacrylonitrile and its TiO_2 composites were electrospun into nanofibers in N, N'-dimethylformamide for photocatalysis and antifouling experiments. The resultants nanofibers were characterized using field emission scanning microscope, Fourier transform infrared spectroscopy, x-ray diffraction, x-ray photoelectron spectroscopy and contact angle analyses. Fourier transform infrared spectroscopy confirmed the formation of polyacrylonitrile-TiO_2 composite nanofibers with their diameter ranging from 10 to 340 nm. The x-ray photoelectron spectroscopy results indicate the formation of O–Ti–C bonds on polyacrylonitrile-TiO_2 matrix. polyacrylonitrile-TiO_2 and polyacrylonitrile nanofiber surfaces showed superhydrophobicity with water contact angle of 155 ± 1 and 154 ± 1, respectively at 120 s. The photocatalytic properties of polyacrylonitrile nanofibers and polyacrylonitrile-TiO_2 nanofibers were investigated under a simulated visible light source of 1000 W/m^2 using methylene blue. About 90% of methylene blue was degraded within 3 h of exposure using polyacrylonitrile-TiO_2 nanofibers while 55% methylene blue degradation was achieved for polyacrylonitrile nanofibers. Photoluminescence experiment conducted on both materials showed that polyacrylonitrile-TiO_2 could produce OH radicals 10-fold compared to polyacrylonitrile nanofibers. Antimicrobial tests were conducted using *E. coli* and *Bacillus* sp. The results showed that only polyacrylonitrile-TiO_2 under visible light hindered the growth of these bacteria with a greater effect on the Gram-positive bacterium, *Bacillus* sp. The photo-degradation and microbial growth inhibition properties of polyacrylonitrile-TiO_2 showed that the material could be used as an antifouling material under visible light.

1. Introduction

Wastewater is full of contaminants, such as organic and inorganic compounds, bacteria and their toxins. Membrane processes are one of the key components of wastewater reclamation [1]. In membrane treatment of wastewater, the problem of fouling arises. Fouling includes accumulation of chemical molecules (chemical fouling) and biological organisms (biofouling) on the membrane. The fouling could be because of macro organic compounds, or organisms, or both depending on the application of the membrane. One major organic foulant is dye molecules. Dye molecules tend to accumulate over time and eventually block the membrane. Fouling of membranes by dye molecules is a major problem to resolve in textile industries [2,3]. In marine industries, however, biofouling is recognized as a threat as it affects the economy and the functionality of equipment [4]. Biofouling is defined as the accumulation or adsorption of micro- or macro-organisms on surfaces of materials [5,6]. Unlike dye molecules that can be removed using low pH feed water, biofoulants are so recalcitrant that when they are removed

* Corresponding authors at: Department of Marine Science and Fisheries, Sultan Qaboos University, 123 Al-Khoud, PO Box 34, Muscat, Oman (S. Dobretsov).
E-mail addresses: cbode-aluko@uwc.ac.za (C. Ademola Bode-Aluko), sergey@squ.edu.om (S. Dobretsov).

https://doi.org/10.1016/j.mseb.2020.114913
Received 19 February 2020; Received in revised form 30 September 2020; Accepted 21 October 2020
Available online 9 November 2020

by pre-treatment of the feed water, there are still enough microbes left to grow by utilizing biodegradable substances [5]. Altogether, the impact of fouling leads to significant economic impacts, with previous work estimating the costs of biofouling and biofouling control to be as high as 30% of the plant's total operating costs [7,8]. Fouling has been tackled with methods such as surface coatings (using antifouling materials) and surface modification (changing the surface chemistry of the membrane) so as to reduce the adhesion of foulants [5,6]. Finding a benign and self-cleaning material becomes imperative. Researchers have made several efforts in finding materials with such properties. For instance, polymers have been reported for developing antifouling coatings [9].

Removal of organic pollutants such as methylene blue [3,10,11] has been widely report in literature, using methods such as; sedimentation, chemical treatments, electrochemical methods, advanced oxidation processes, biological treatments, membrane filtration, adsorption and ion exchange [3,12]. Apart from the fact that some of the methods require the use of chemicals, two or more of them have to be combined for better removal results [3,12]. Meanwhile, in the past few decades, researchers have also been looking into the advantages of solar energy in water remediation technologies such as advanced oxidation processes (AOP) [13]. AOPs are based on the generation of oxidizing agents such as the hydroxyl radicals that can attack many pollutants present in waters [14]. The production of hydroxyl radicals could be initiated by an electric field, ultrasound or by light irradiation. Therefore, in the presence of a catalyst, the light energy coming from the sun could be used as an initiator in the production of the hydroxyl radical. This process is known as photocatalysis.

In literature, photocatalytic method has shown excellent antifouling results on bacteria [15–17] and degradation of methylene blue [10,11]. Amongst photocatalytic materials, stands out as the most widely used due to its chemical stability, ability to adsorb electrons, acceptable band gap, affordability and environmentally friendliness [12,13,18]. Many studies have used TiO_2 in waste water management and solar energy harvesting. TiO_2 is used in breaking down most organic pollutants such as dyes, pesticides and herbicides under light irradiation [12]. The challenge in most cases is recovering of the TiO_2 from the treated water. Therefore, researchers have made composites of TiO_2 and nanofibers for applications such as removal of heavy metals [19], for photocatalytic degradation [20,21] and as anti-fouling membranes [22,23]. Other photocatalytic materials that have been reported include C_3N_4, ZnO, ZnS, $SrTiO_3$ and CdS [15,24]. Generally, these nanocomposite materials absorb light during photocatalysis leading to promotion of electrons from their valence band to their conduction band, leaving a hole in their valence band resulting to photo-redox reaction. However, most of the materials experience recombination of generated photo electrons thereby reducing their photocatalytic ability [11,15]. To mitigate this effect, catalysts are modified using methods such as doping with metals/nonmetals and coupling with carbon materials [24] to act as sinks for the generated photo electrons [25].

Polymer nanofibers have been reported to serve as support for catalysts and other biological important compounds either by surface immobilization or as composites [26]. The electrospinning process has been the main nanotechnology method use in fabrication of polymer fibers with diameters in the nanometer range. At these diameters, nanofibers exhibit characteristics such as high surface area to volume rate. Electrospinning can produce polymer nanofibers in a continuous mode [27–30]. Other methods such as self-assembly, chemical vapor deposition, template-assisted synthesis and wet chemical synthesis have also been used to produce nanofiber materials, however, electrospinning possess advantages such as allowing easy doping, simplicity, low cost, and high reproducibility [31]. Polymers that have been successfully electrospun into nanofibers include; polyamide 6, polyacrylonitrile, polyethylene terephthalate, polystyrene etc. [32–34]. Among these polymers, polyacrylonitrile stands out due its excellent characteristics such as high carbon content, chemical resistance, good thermal stability and superior mechanical properties [27,35].

This study investigated the use of polyacrylonitrile nanofibers as support for TiO_2 catalyst in the development of photocatalytic and antifouling materials. The aim was to develop visible light photocatalytic nanofibers to control fouling by organic molecules (methylene blue) and microorganisms (*E. coli* and *Bacillus* sp.).

2. Materials and methods

2.1. Materials

Polyacrylonitrile (PAN) (Ave. Mw = 150000 g/mol) was purchased from Sigma, South Africa while N, N'-dimethylformamide (DMF) (99.5%) and Degussa Titanium Dioxide nano-powder (particle size 20 nm) was purchased from Kimix, South Africa. Methylene blue and terephthalic acid were obtained from Sigma Aldrich (USA).

2.2. Electrospinning of PAN nanofibers

Electrospinning was conducted according to Bode-Aluko et al. [36]. 8 wt% of PAN was prepared in DMF and was electrospun by introducing the polymer solution into a 20 mL syringe with 0.2 mm inner diameter stainless steel needle. The syringe was fitted into a metering syringe pump. A stationary collector covered with A4 size aluminum foil was used. For the process parameters: the flow rate was set at 0.4 mL/h, and a voltage of 25 kV was applied across the collection distance of 15 cm at a room temperature of 28 °C. The resultant nanofibers were labelled as PAN-nfs (Polyacrylonitrile nanofibers). Similarly, 3 wt% of TiO_2 was mixed with 8 wt% PAN solution in DMF and stirred overnight to form a homogenous solution. The resultant solution was electrospun into nanofibers with the same electrospinning parameters as above to give PAN-TiO2. Further TiO_2 loading (wt%) concentrations were not studied as the homogenous solution could not be electrospun due to high viscosity and also to keep the reactive radical minimal to avoid degradation of the polymer nanofibers.

2.3. Antifouling tests

For this experiment, methylene blue (MB) and bacteria were used to investigate the antifouling properties of PAN-nfs and PAN-TiO2. A solar simulator (Model SS 1.6 kW, Sciencetech Inc., London, ON, Canada) generating air mass 1.5 (AM 1.5) illumination of solar spectra of 1000 W/m^2 was used to conduct photocatalysis experiments with methylene blue and bacteria.

2.4. Degradation of methylene blue

First, the nanofiber mat size of dimension 1 cm × 3 cm was soaked overnight in 3 mL of 10 ppm MB in order to determine the adsorption capacity and the time to saturate each membrane in the dark. The presoaked PAN-nfs or PAN-TiO_2 nanofibers were removed and dried at room temperature without washing. The photocatalysis experiments were conducted using a solar simulator for 3 h. For this, the dried presoaked nanofibers were incubated in 3 mL of 10 ppm MB. The resultant concentrations of MB were analyzed using UV–Vis spectroscopy (Ocean Optics, USA) over wavelength range 400–800 nm at every 30 min.

2.5. Antimicrobial experiment

In this experiment, the Gram-negative fresh water bacterium *Escherichia coli* (ATCC 25922) and Gram-positive marine bacterium *Bacillus* sp. isolated from a desalination plant were used. Prior to the experiment, *E. coli* was cultured using nutrient broth (Sigma, USA), while *Bacillus* sp. was cultured in marine broth (Difco, Fisher Scientific, USA). Both strains were maintained at 37 °C for 24 h. The antimicrobial experiment was conducted according to Al-Fori et al. [37]. Briefly,

cultures were centrifuged and re-suspended in fresh broth to obtain an absorbance of 0.1 (at 620 nm). Each well of a 24-well plate (Nunc) contained 2.5 mL of bacterial culture and pieces (1 cm^2) of PAN-nfs or PAN-TiO2. As the control, wells with 2.5 mL of bacterial culture were used. The experiment was conducted for 48 h at 37 °C under light (using the solar simulator) and dark (covered with aluminum foil) conditions. After 24 h and 48 h, the optical density (at 620 nm) of the bacterial culture was measured using a multi-well plate reader (Thermo Scientific Multiskan, USA). The number of viable *E. coli* cells in samples under light conditions was estimated using a serial dilution technique. All samples were tested in triplicate.

2.6. Production of OH radicals

In order to investigate the behavior of materials in terms of photocatalysis, their abilities to produce OH* radicals were studied. Chemical dosimetry based on terephthalic acid (TA) was used to measure the OH radicals produced during photocatalysis. TA is a well-known scavenger which does not react with other radicals except OH* radicals [38]. As shown in reaction scheme 1, the OH* radical can convert non-fluorescent TA to fluorescent 2-hydroxyterephthalic acid (HTA). Therefore, during irradiation of a solution containing TA and HTA molecules, HTA molecules will emit light at λ = 425 nm, while TA molecules will not.

$$C6H4(COOH)2 + \cdot OH \rightarrow C6H4(COOH)2OH \quad (1)$$

Reaction scheme 1: Conversion of Terephthalic acid to 2-hydroxyterephthalic acid.

Prior to the experiment, an aqueous solution of 0.25 mM TA was prepared in 200 mL aqueous solution of 2 mM NaOH. PAN-nfs or PAN-TiO_2 of 2 cm^2 were cut and placed in 25 mL of TA solution. Then, the solution with samples was placed under the solar simulator at 1000 W/m^2. The emission was measured at every 15 min for 3 h using Photoluminescence spectrometer (PerkinElmer LS 55, USA). The excitation wavelength was set at 315 nm, and the fluorescence spectra of each experiment were collected from 340 to 625 nm. The fluorescence spectrum around

λmax = 425 nm (peak of interest) was plotted as photoluminescence intensity against wavelength

2.7. Characterization

The surface morphology of PAN-nfs and PAN-TiO_2 was characterized by Field Emission Scanning Microscope (FESEM, JEOL JSM-7800F, Japan). Working voltage and distance were maintained at 5 kV and 10 mm during measurement. The average fiber diameter (AFD) in SEM images was determined using Image J software. The X-ray diffraction (XRD) machine (Rigaku Miniflex 600, Tokyo, Japan) working at 40 kV, 15 mA was used to observe the amorphous nature of PAN-nfs and the presence of TiO_2 in its composite.

Fourier Transform Infrared Spectroscopy attached with attenuated total reflection (Perkin Elmer, USA) was used to examine the surface functional groups of PAN-nfs and PAN-TiO_2 in the 400–4000 cm^{-1} range with a signal resolution of 4 cm^{-1}. X-ray photoelectron spectroscopy (XPS) was performed using multi-probe photoelectron spectroscopy (Omicron Nanotechnology, Germany) with a monochromatic Al Kα excitation (hν = 1486.6 eV) working at 15 kV with emission current of 20 mA. Pass energy of 50 eV was used for the survey scan and 20 eV for the high resolution scan. Acquired spectra were analyzed by using CASA XPS software with Shiely function background and Gaussian-Lorentzian function (0.3 * Gaussian + 0.7 * Lorentzian) (Casa Software Ltd, UK). Since the low quantity of Ti (~1.44%: estimated from the XPS survey spectrum) on the PAN nfs/TiO_2 surface, Ti 2p peak was not seen clearly in the original data. Therefore, the SG Quadratic function (smoothing width = 5) was introduced on the original obtained data by averaging in Casa XPS software [39]. Intrinsic carbon peak (C–C/C–H) at 284.6 eV was used as calibration reference.

The sample's hydrophilicity/hydrophobicity was determined by measuring the static contact angle of a water drop on the membrane with Theta Lite attention tensiometer (Biolin Scientific, Sweden) using the sessile drop technique. All the measurements were carried out at room temperature at time interval of 0 – 120 s. Deionized water with volume of 5 μL was used as test liquid and the measurement was repeated three times and the average value was reported.

3. Results and discussion

3.1. Characterization of PAN-nfs and PAN-TiO2

The FESEM images (Fig. 1 (a) and (b)) show that PAN-nfs and PAN-TiO_2 surfaces were smooth without the presence of beads. The diameter and size distribution of fibers were determined using Image J software (NIH, USA) and the results showed that PAN-nfs had diameters ranging from 70 to 230 nm and PAN-TiO_2 had diameters of 110 – 340 nm respectively (See Fig. 1c and d).

The mean diameter of PAN-nfs was found to be around 140–170 nm and PAN-TiO_2 fibers were around 160–210 nm. PAN-TiO_2 fiber had bigger diameter and wider range than PAN-nfs, which might due to the inclusion of TiO_2 that affected the fiber diameter during the fabrication process. In PAN-TiO_2 sample, TiO_2 particles were presented in an aggregated fashion on the fiber surface (See Fig. 1b inset). The formation of the aggregation has been previously reported [40].

The ATR-FTIR spectrum (Fig. 2a) of the PAN-nfs has the following characteristic peaks that are unique to PAN; the peak at 2924 cm^{-1} is assigned to C–H stretching vibration of CH2 and the peak at 2241 cm^{-1} corresponded to the C≡N stretching vibration. The strong bands at 1450 cm^{-1}, 1345 cm^{-1} and 1220 cm^{-1} can be assigned to the aliphatic CH group vibrations of CH2 groups. The appearance of a peak at 1728 cm^{-1} on PAN-nfs which corresponds to the C═O stretching vibration is assumed to have come from the C═O of methacrylate [41]. Similarly, the spectrum of PAN-TiO_2 shows the same peaks except the appearance of broad band at 850–550 cm^{-1} and the weakened bond strength of C═O suspected to be due to the metal coordination [42] which was further confirmed by XPS. The band is characterized as the vibrations of Ti–O and Ti–O– Ti framework bonds.

The X-ray diffraction (XRD) analysis was carried out to check the change in the amorphous phase of PAN-nfs before and after incorporation of TiO_2 (Fig. 2b). For PAN-nfs, a strong diffraction peak centered at 17.3° corresponds to the hexagonal lattice and a weak diffusion peak centered at 27.2° was observed [43]. For, PAN-TiO2, the sharp diffraction peaks at 25.1° and other minor peaks at 37.7°, 47.8°, 53.7° and 62.4° were attributed to (101), (004), (200), (105) and (204) planes in TiO_2 anatase mineral phase [44]. An indistinct phase was also detected at 27.2° and could be assigned to (110) plane of rutile TiO_2 [45]. A peak at 17.3° was also observed in PAN-TiO_2 but at low intensity due to the suppression from TiO_2 peaks.

In order to verify the elemental composition and surface chemistry of PAN-nfs and PAN-TiO2, XPS analysis was carried out (Fig. 3). Survey spectra shows three core level peaks of C 1 s, N 1 s and O 1 s obtained from PAN-nfs and PAN-TiO_2 [46–48]. A small extra peak was detected on PAN-TiO_2 sample at 457 eV and 463 eV which correspond to the Ti 2p3/2 and Ti 2p1/2 with a spin orbit splitting of ~ 6 eV (Fig. 3a inset). Fig. 3b and c show high resolution XPS spectra of core-level C 1 s peaks for PAN-nfs and PAN-TiO2. C 1 s spectra for PAN-nfs can be deconvoluted into three components where C–C/C–H at 284.6 eV [48], C≡N at 286.1 eV and C═O at 288.4 eV respectively. From literature, the binding energies for C≡N was reported at 286.4, 285.9, 286.6 eV [49–51] and for C═O at 288.6, 288.5, 288.5 eV [52–54] where our results are in good agreement with those reported values. In the case of PAN-TiO_2 (Fig. 3c), the binding energies at 284.6 eV and 285.9 eV can be attributed to C–C/C–H bonds and C≡N bonds (slight shifting of BE ~ 0.2 eV). A new feature appeared at 283.4 eV on PAN-TiO_2 sample, which could be

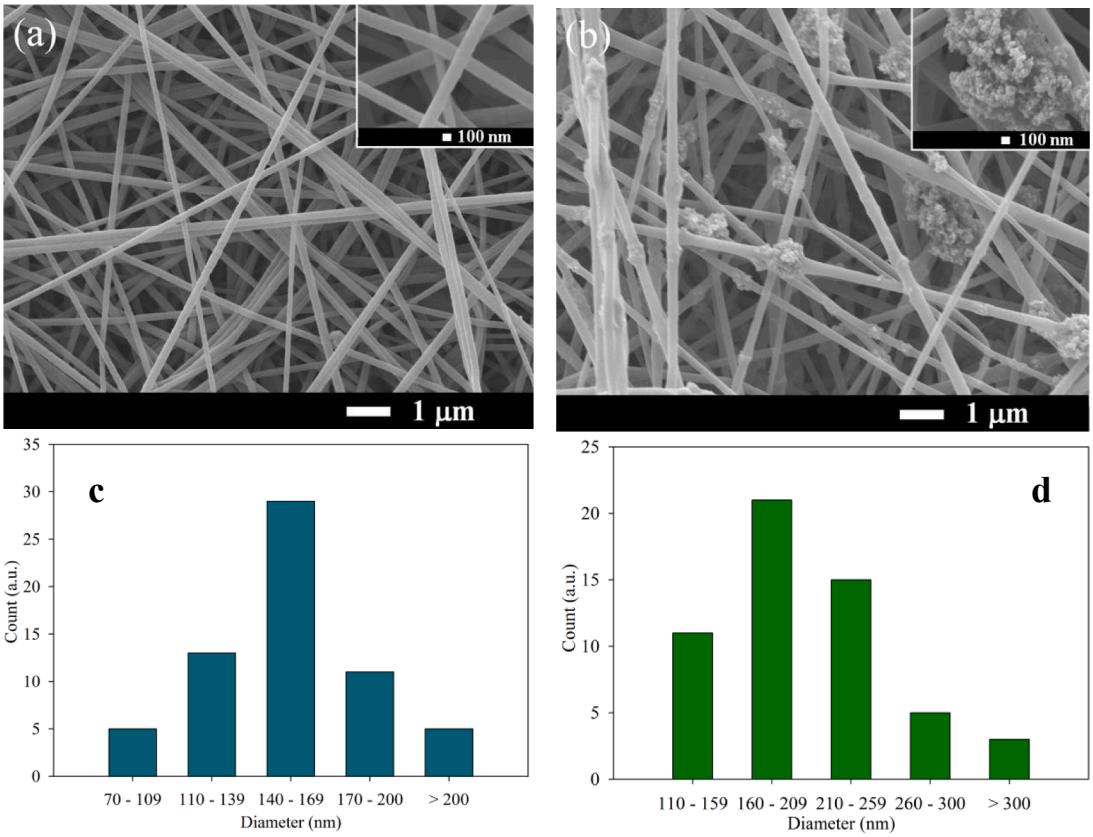

Fig. 1. (a) FESEM image of PAN-nfs (Inset shows high magnification image of nanofiber), (b) FESEM image of PAN-TiO2 (Inset shows high magnification image of TiO2 nanoparticles aggregated embedded in nanofiber) (c) Size distribution of PAN-nfs fiber and (d) Size distribution of PAN-TiO2 fiber.

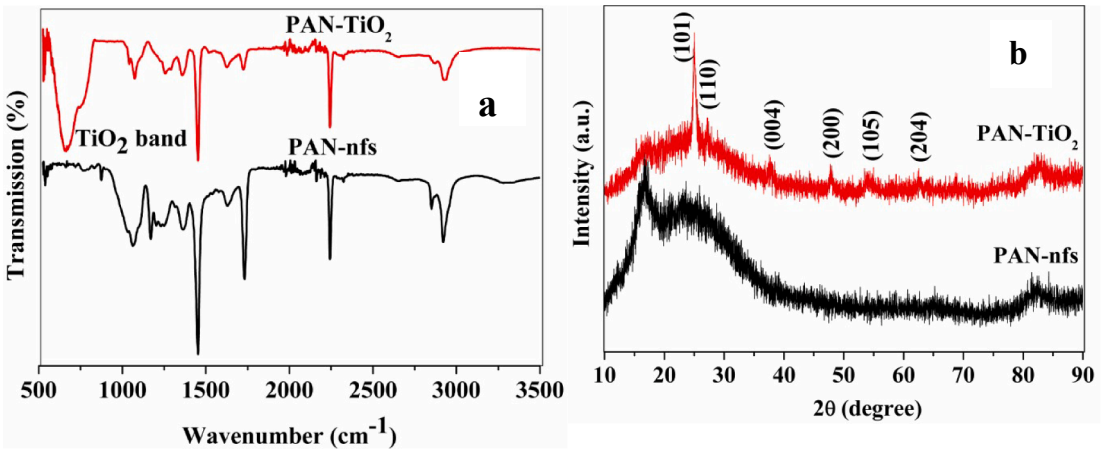

Fig. 2. (a) ATR-FT-IR spectra of PAN-nfs and PAN-TiO2 and (b) XRD pattern of PAN-nfs and PAN-TiO_2.

ascribed to O–Ti–C bonds [48]. The amount of C–C/C–H was reduced substantially from 89.2% to 71.8% and a slight reduction of C≡N ca. 2% were due to the formation of O–Ti–C bonds while TiO_2 nanoparticles were incorporated in polyacrylonitrile matrix. Moreover, slightly lower binding shifting (ca. 0.2 eV) of N 1 s peak in PAN-TiO_2 sample compared with PAN-nfs suggested the interaction between nanofibers and TiO_2 nanoparticles. The C═O feature was completely diminished in PAN-TiO_2 sample which can also be observed in FTIR (Fig. 2a). O 1 s peak of PAN nfs comprises of two distinct peaks centred at 530.6 eV and 526.3 eV (Fig. 3d). Typically, BE value at 530.6 eV can be assigned to lattice oxygen related bonding where 526.3 eV probably can be assigned to some carbon containing doping [55]. After incorporating the TiO_2 nanoparticle, core level O 1 s peak on PAN nfs/TiO_2 surface has left with single peak located at 530.6 eV (Fig. 3e).

The X-ray diffraction pattern of PAN-TiO_2 clearly indicates the formation of intense Ti diffraction peaks. However, in XPS spectra, Ti peaks both in wide survey and high resolution scans are very feeble and noisy due to low quantity of Ti (~1.44%: estimated from the XPS survey spectrum) on the PAN-TiO_2 nfs surface. In addition, XPS is a unique surface-sensitive technique that detected electrons originate only from the top few nanometer (~10 nm) while XRD technique can verify the crystalline materials within ~ 10 µm of the surface. Therefore, the noisy and very feeble XPS peak is due to the lack of exposure of Ti on the PAN-Nfs surface (some portions of TiO_2 nanoparticles are embedded in fiber

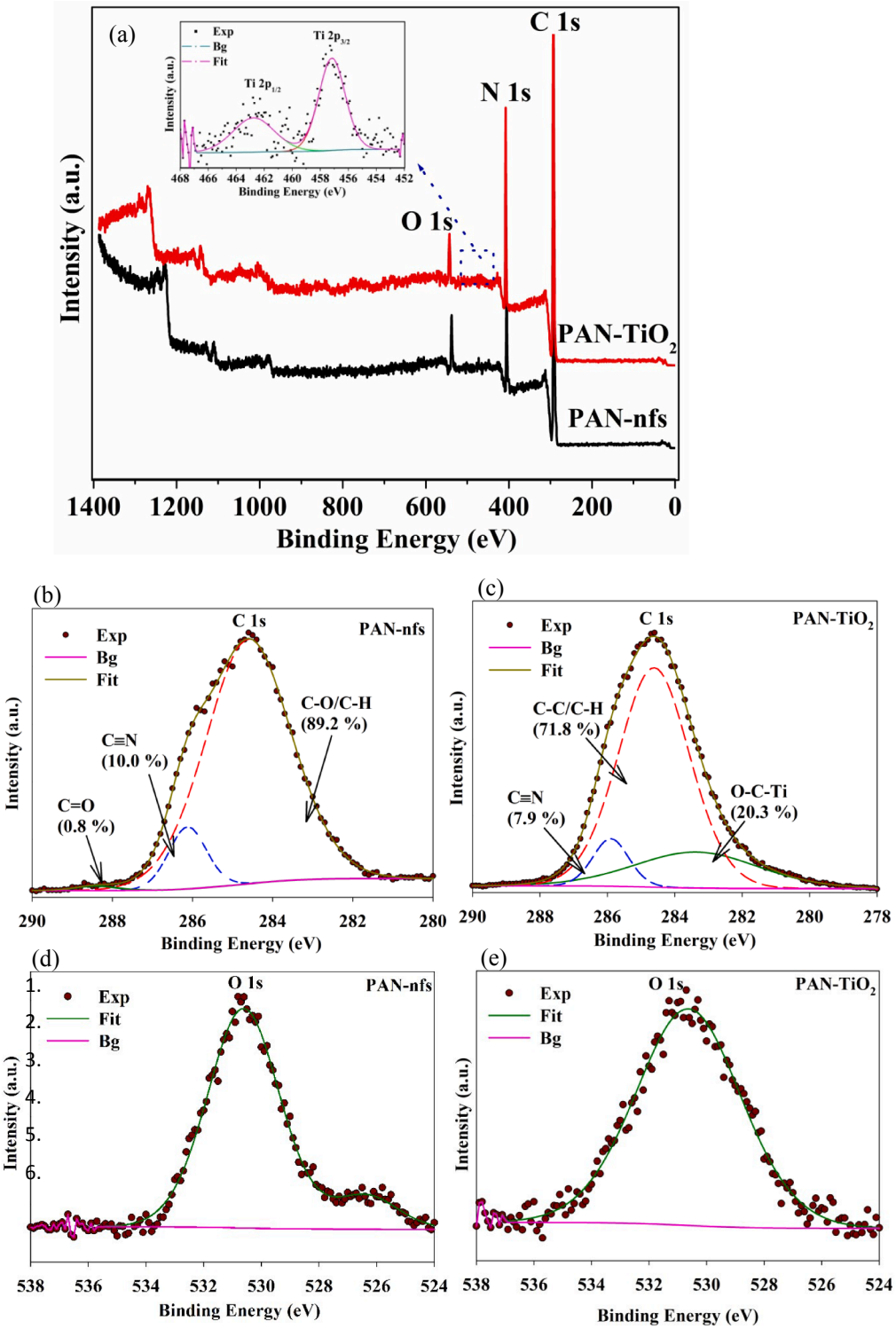

Fig. 3. (a) XPS survey spectra of PAN-nfs and PAN-TiO2 (inset shows Ti 2p), high resolution XPS spectra of C 1 s for (b) PAN-nfs and (c) PAN-TiO2 (d) O1s high resolution of PAN-nfs and (e) O1s high resolution PAN-TiO_2.

matrix) that reduces the intensity of Ti2p peak.

Table 1 shows the estimated atomic relative concentration of individual element such as carbon, oxygen, nitrogen and titanium on PAN-nfs and PAN-TiO_2 sample surfaces.

Surface wetting results of PAN-nfs and PAN-TiO_2 are shown in Fig. 4. Initially, both surfaces showed superhydrophobicity with water contact angle (WCA) of 155° ± 1°for PAN-nfs and 154° ± 1°for PAN-TiO_2 respectively (Fig. 4a and 4c). However, the PAN-nfs surface could not

Table 1
The estimated atomic relative concentration of carbon, oxygen, nitrogen and titanium on PAN-nfs and PAN-TiO2 samples surface.

Type	atomic%				
	C1s	O1s	N1s	$Ti2p_{3/2}$	$Ti2p_{1/2}$
PAN-nfs	78.23	4.74	17.03	–	–
PAN-TiO_2	72.95	3.39	22.23	0.46	0.98

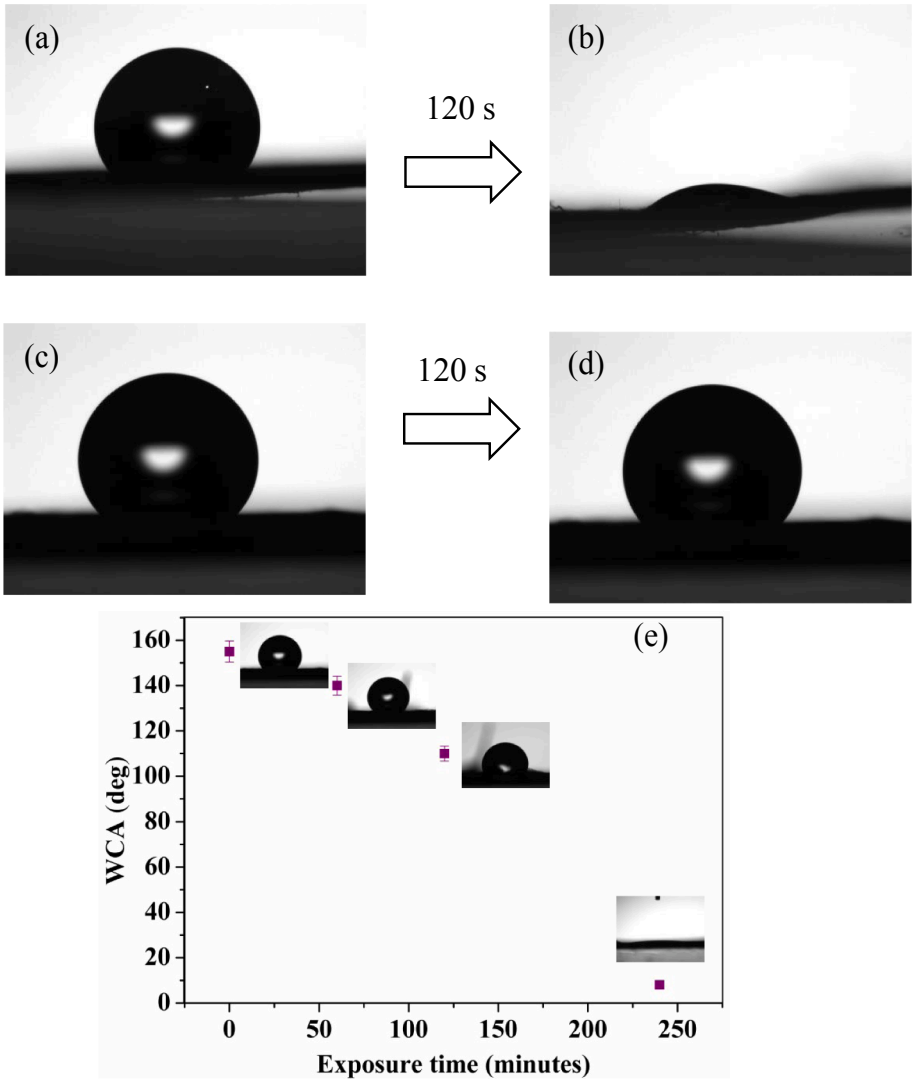

Fig. 4. Optical images of 5 μL droplet sits on (a) PAN sample surface, (b) PAN sample surface after 120 s, (c) PAN-TiO2 sample surface, (d) PAN-TiO2 sample surface after 120 s, (e) Water contact angle changes with respect to visible light exposure time on PAN-TiO2 surface.

sustain their superhydrophobic nature thus the WCA dropped from 155 ± 1°to 25 ± 3°after 120 s (Fig. 4b). Conversely, PAN-TiO2 surface maintained its superhydrophobic nature after 120 s (Fig. 4d).

120 s

In order to understand how surface wetting plays an important role on photodegradation and antimicrobial activities, the surface wetting nature of PAN-TiO2 was studied under exposure of visible light. Fig. 4e shows the transformation of superhydrophobic (WCA ~ 155°) to super hydrophilic (WCA ~ 8°) nature of PAN-TiO2 surface by constant exposure of visible light over 4 h. It is a well-known phenomenon that semiconductors such as TiO2 or ZnO can be transformed from being hydrophobic to hydrophilic by irradiation of ultra-violet light or visible light [56]. In our case, visible light (1000 W/m^2) was used and a longer exposure time was needed to render the surface superhydrophilic. This could be due to the low content of TiO2 in the fiber matrix which could turn the surface hydrophilic.

3.2. Photoluminescence tests

To further investigate generation of OH* radicals by PAN-nfs or PAN-TiO2 under visible light, photoluminescence (PL) measurements using terephthalic acid (TA) were carried out. Fig. 5a and 5b show the PL spectral of hydroxyterephthalic acid solution under visible light obtained at different times in the presence of PAN-nfs and PAN-TiO2, respectively.

During photocatalysis, photocatalyst produced OH* radicals, which reacted with non-fluorescent TA to produce highly fluorescent 2-hydroxyterephthalic acid [38]. 2-hydroxyterephthalic acid can be detected by a spectrophotometer the PL peak λmax at 425 nm. Comparison of the rate of production of OH* radicals from PAN-nfs and PAN-TiO2 showed that at the same initial concentration of TA, PAN-TiO2 produced much higher amount of OH* radicals compared to PAN-nfs. The saturation for PAN-TiO2 was reached (PL intensity 1000) after 135 min, while for PAN-nfs was still at PL intensity 80 after 180 min. This experiment proves our hypothesis that PAN-TiO2 produces OH* radicals and the observed activity is due to free radicals formed by photocatalysis.

During photocatalysis, photocatalyst produced OH* radicals, which reacted with non-fluorescent TA to produce highly fluorescent 2-hydroxyterephthalic acid [38]. 2-hydroxyterephthalic acid can be detected by a spectrophotometer the PL peak λmax at 425 nm. Comparison of the rate of production of OH* radicals from PAN-nfs and PAN-TiO2 showed that at the same initial concentration of TA, PAN-TiO2 produced much higher amount of OH* radicals compared to PAN-nfs. The saturation for PAN-TiO2 was reached (PL intensity 1000) after 135 min, while for PAN-nfs was still at PL intensity 80 after 180 min. This experiment proves our hypothesis that PAN-TiO2 produces OH* radicals and the

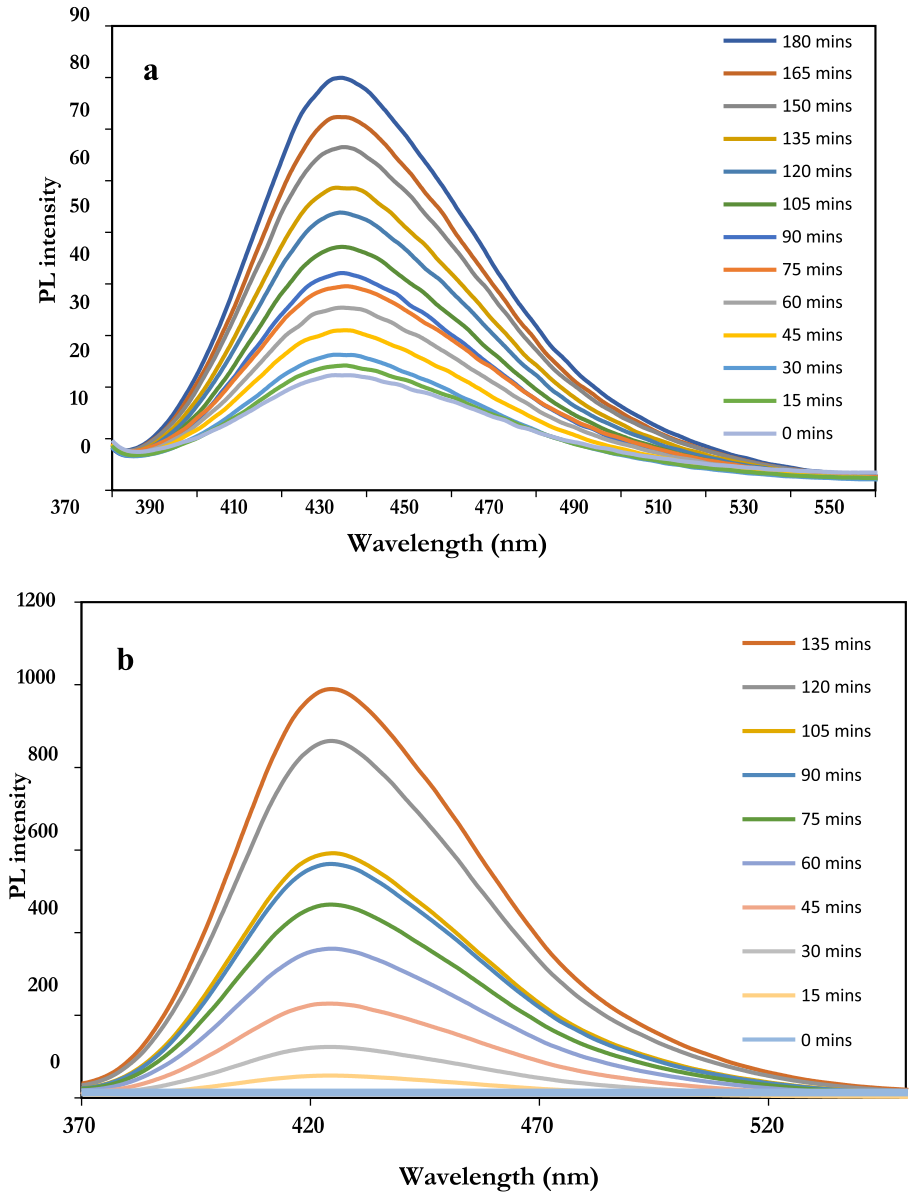

Fig. 5. PL spectra of conversion of non-fluorescent terephthalic acid to fluorescent 2-hydroxyterephthalic acid (HTA) as a result of OH radicals generated using (a) PAN-nfs and (b) PAN-TiO_2.

observed activity is due to free radicals formed by photocatalysis.

3.3. Photodegradation of MB

The photo-degradation of MB was studied using PAN-nfs and PAN-TiO2 under visible light (Fig. 6). Both nanofibers can adsorb MB, but adsorption was not significant in the absence of light (Fig. 6a and 6b). For light experiments, the lower absorbance is mainly due to degradation. Under visible light, PAN-TiO2 shows about 90% while PAN-nfs about 55% of dye degradation after about 3 h (Fig. 6c). After the first 30 min, degradation of MB on PAN-nfs is slightly higher than PAN-TiO2 due to the hydrophobic nature of PAN-TiO2 surface (WCA ~ 150° which is not shown in Fig. 4d). However, after 60 min or more PAN-TiO2 surface turns hydrophilic (See Fig. 4e) which then results in faster degradation rate (See Fig. 6c). This turning point can be observed from the high production of OH* radical after 100 min of exposure time (See Fig. 5b). About 2% of MB degraded in the control as well. This is probably due to dye bleaching under the light [57,58].

PAN-TiO2 was 2-fold more effective in MB dye degradation compared to PAN-nfs. The liberation of OH* radicals as a result of photo-irradiation could have initiated reactions leading to MB degradation [59]. The results showing that the PAN-TiO2 has the highest degradation were probably due to higher production of OH* radicals by TiO2. Photocatalytic degradation of MB by TiO2 under visible light was reported earlier [60–63]. The result reveals that TiO2 containing PAN-based fibers could be applied for environmental remediation with self-cleaning properties under visible light. PAN-nfs by themselves showed some photocatalytic activity under visible light irradiation. This is perhaps an emerging characteristic of polymers, as polymers such as polyethersulfone, have shown photocatalytic properties [59,63]. Dye removal could be ascribed to physical adsorption of the dye onto the PAN-nfs but the production of free radicals shown in Fig. 6 argues otherwise.

TiO_2 nanoparticles mainly absorb UV light due to its wide band gap, however, their photocatalytic effect on MB and biofouling under visible light could be due to sensitization mechanism [64–66]. In case of dyes, instead of TiO_2, the dye molecules absorbed visible light, got excited and transferred the electrons into the conduction band of TiO_2 leading to

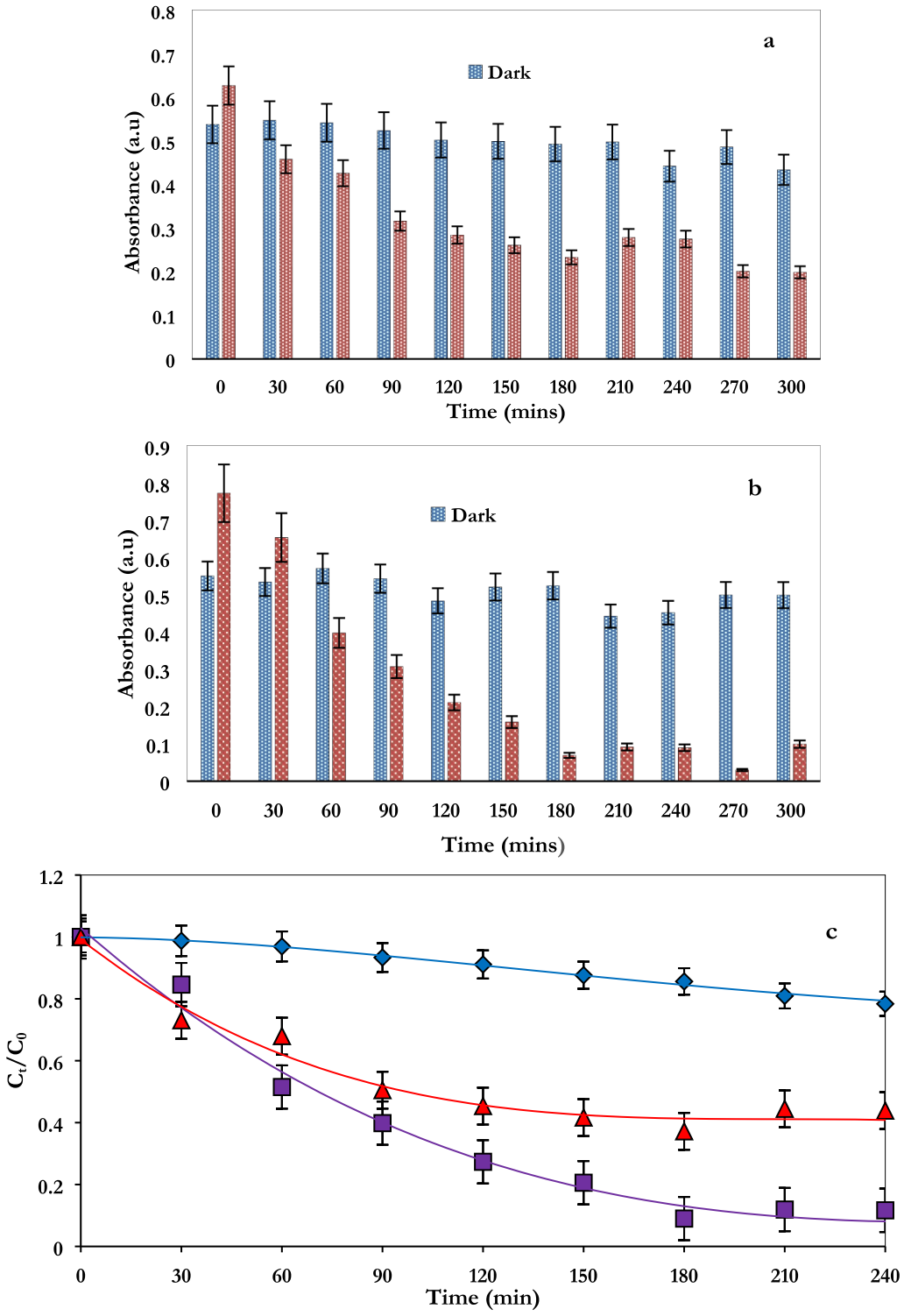

Fig. 6. The results of the dark and light experiments for degradation of MB using PAN-nfs (a) and PAN-TiO2 (b), and (c) kinetic degradation of MB under visible light.

formation of radicals [64–66]. Moreover, the sensitization could have also come from PAN-nfs as polymer-sensitizer of TiO_2 has been previously reported [65], therefore, PAN-nfs may have served as the organic sensitizer that absorbed the visible light.

3.4. Antimicrobial test

Previously, electrospun PAN fibers modified with silver nanoparticles were shown to have excellent antibacterial properties [67,68]. At the same time, the antimicrobial properties of PAN-TiO2 have not been investigated so far. In this study, we studied the antimicrobial properties of PAN-nfs and PAN-TiO2 in the dark and light experiments. The experiments were conducted using a common human bacterial pathogen *E. coli* [69]. This is a Gram-negative bacterium associated with the lower intestine of humans. Some strains of this bacterium cause serious diarrhea and food poisoning in humans [70,71]. Our experiments showed that there was no significant difference between optical densities of *E. coli* cultures in the dark experiment with PAN-nfs and

PAN-TiO2 (Fig. 7a). On the contrary, at the light conditions PAN-TiO2 inhibited 3-fold the growth of bacteria compare to PAN-nfs and the control (only bacteria) after 24 h. The number of viable bacteria expressed as colony forming units (CFU) was 10-fold lower in treatments with PAN-TiO2 (1.4×10^8 CFU/ml) compared to that with PAN-nfs (18.4×10^8 CFU/ml). However, after 48 h to exposure of visible light, the density of bacteria in the presence of PAN-TiO2 was similar to the control sample but 2-fold lower than in the presence of PAN-nfs (Fig. 7a). This could be explained by enhanced cell growth of *E.coli* on hydrophilic surface of PAN-nfs.

Similarly, in the visible light experiment PAN-TiO2 inhibited the optical density of Gram-positive biofouling bacterium *Bacillus* sp. (Fig. 7b). Since PAN-TiO2 inhibited growth of *E. coli* as well, this suggests that PAN-TiO2 fibers have potent antimicrobial properties against Gram-negative and Gram-positive bacteria. The reduction of the number of bacteria can be explained by two hypotheses. First, bacteria can be killed due to production of reactive oxygen species during photocatalysis. Second, bacteria can accumulate on the surface of the fibers. Our data suggested that most likely bacteria were eliminated due to photocatalysis as we would not observe a dramatic reduction of viability of bacteria in the case of adsorption of bacteria especially for Gram positive bacteria. Under the dark condition, PAN-TiO2 sample showed slight reduction of bacterial density compared with the control sample (bacteria only). This might be due to: (1) slight adsorption of bacteria on the PAN-TiO2 surface and (2) slow release of catalytic ions into the media, which inhibit the bacteria growth.

Photocatalytic inhibition of *E. coli* growth by TiO2 has been shown previously. For example, Egerton et al. [71] demonstrated the possibility of photoelectrocatalytic disinfection of *E. coli* by an iron doped TiO2 sol–gel electrode. A linear relationship between the concentration of OH* radicals and inactivation of *E. coli* by TiO2 photocatalysis has been shown [72]. Novel ZnO-TiO2 composite nanofibers were fabricated by an electrospinning method and showed excellent antimicrobial activity against Gram-negative *E. coli* and Gram-positive *Staphylococcus aureus* bacteria under UV light [73]. However, our research showed that PAN-TiO_2 showed greater effect on the Gram-positive bacterium, *Bacillus* sp. under visible light.

4. Mechanism of antifouling action

The proposed mechanism of antifouling activity of PAN-TiO2 fibers against chemical and biological fouling is due to photocatalytic activity and production of reactive oxygen species under visible light. When PAN-TiO2 fibers are exposed to visible light in the aquatic environment, multiple electron-hole pairs are generated through bandgap absorption.

This results in the generation of reactive oxygen species (ROS), like

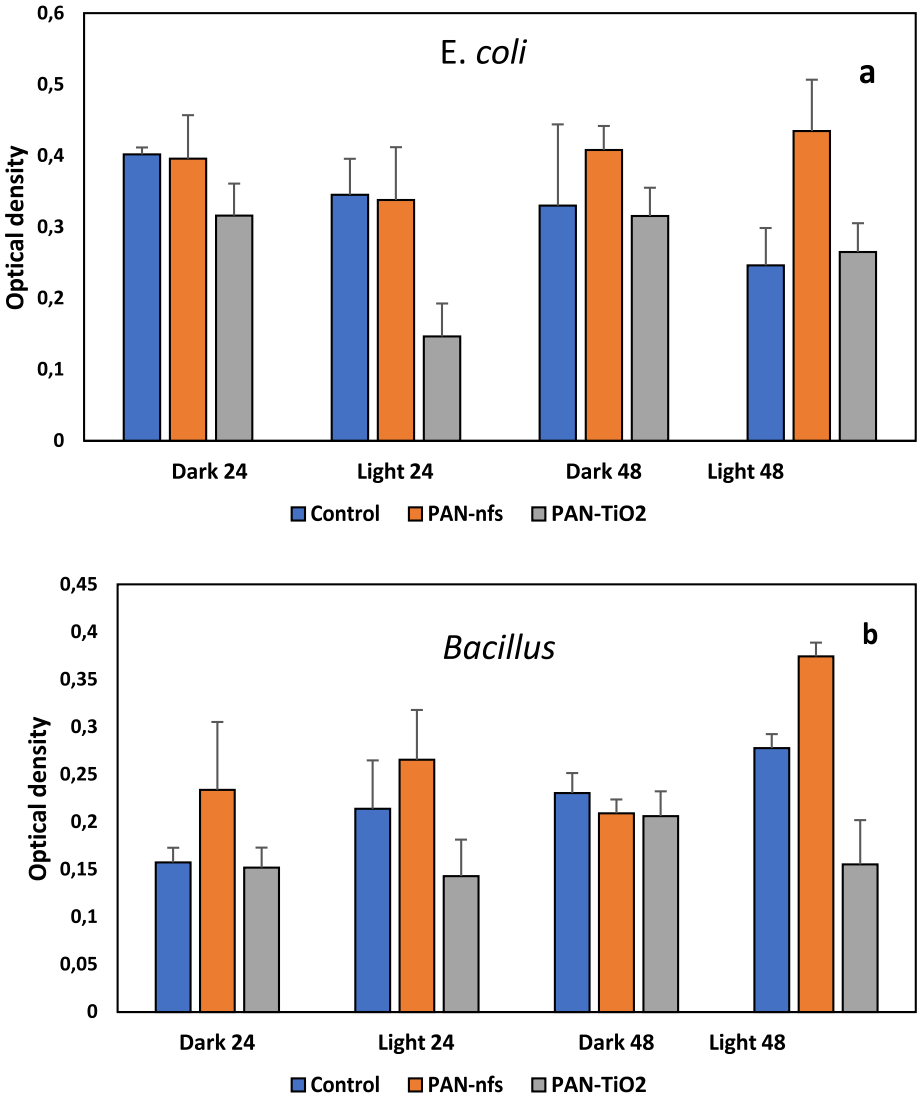

Fig. 7. Optical density (620 nm) of (a) *E. coli* and (b) *Bacillus* sp., at 24 and 48 h under dark and light. The control contains wells with bacterial culture only. The data are the mean ± standard deviation.

hydroxyl radicals (OH*) and superoxide ions ($O2^{-}$). Radicals can further undergo cascaded reactions with H^{+} and photogenerated electrons (e^{-}) producing peroxides (H_2O_2) and more OH* radicals [6]. These ROS species can oxidize organic molecules, like MB, and kill bacteria. ROS are known to cause cell wall damage and increase cell oxidative stress [74,75]. Additionally, once ROS are inside the cell, they can damage DNA of bacteria and interfere with microbial enzymes and lipids [76,77]. Therefore, PAN-TiO2 fibers can be used for different industrial applications, in which antifouling and self-regenerating activity is required, such as degradation of organic pollutants in industrial water, treatment of produced and wastewater, and disinfection of water. Additionally, PAN-TiO2 fibers can be used as a pre-treatment to reduce fouling of reverse osmosis membranes of desalination plants.

5. Conclusions

In this study, PAN-TiO2 nanofibers were successfully made by a simple electrospinning and blending procedure. High hydrophobicity is imparted to PAN nanofibers by addition of TiO_2, enhancing water repellent properties. In the presence of visible light, these nanofibers showed potent antifouling and photocatalytic activity as well as high hydrophobicity in comparison to unmodified PAN nanofibers. PAN-TiO2 nanofibers successfully removed a dye and killed bacteria within a laboratory experiment. Thus, the antifouling activity and high hydrophobicity of PAN- TiO2 nanofibers could be useful in many industrial applications. Future experiments are needed in order to test the antifouling activity PAN- TiO2 nanofibers in real industrial conditions.

Declaration of Competing Interest

The authors declare that they have no known competing financial interests or personal relationships that could have appeared to influence the work reported in this paper.

Acknowledgment

The authors are grateful to the funder of this research; South African (NRF) - Sultan Qaboos University (SQU, Oman) grant CL/SQU-SA/18/01, OMSA1704413227101.

References

[1] A. Lee, J.W. Elam, S.B. Darling, Membrane materials for water purification: design, development and application, Environ. Sci-Wat. Res. 2 (2016) 17–42.
[2] M. Shah, Effective Treatment Systems for Azo Dye Degradation: A Joint Venture between Physico-Chemical & Microbiological Process, Inter. J. Environ. Bioremed. Biodegrad. 2 (2014) 231–242.
[3] V.K. Gupta, Suhas, Application of low-cost adsorbents for dye removal – A review, J. Environ. Manage. 90 (2009) 2313–2342.
[4] S. Dobretsov, Inhibition and Induction of Marine Biofouling by Biofilms. Springer Series on Biofilms, Springer, Berlin, Heidelberg, 2019.
[5] S.S. Bucs, N. Farhat, J.C. Kruithof, C. Picioreanu, M.C.M. van Loosdrecht, J. S. Vrouwenvelder, Review on strategies for biofouling mitigation in spiral wound membrane systems, Desalination 434 (2018) 189–197.
[6] L. Al-Naamani, S. Dobrestov, J. Dutta, J.G. Burgess, Chitosan-zinc oxide nanocomposite coatings for the prevention of marine biofouling, Chemosphere 168 (2017) 408–417.
[7] D. Rice, A.C. Barrios, Z. Xiao, A. Bogler, E. Bar-Zeev, F. Perreault, Development of anti-biofouling feed spacers to improve performance of reverse osmosis modules, Water Res. 145 (2018) 599–607.
[8] H.C. Flemming, Reverse osmosis membrane biofouling, Exp. Therm. Fluid Sci. 14 (1997) 382–391.
[9] M. Malini, M. Thirumavalavan, W. Yang, J. Lee, G. Annadurai, A versatile chitosan/ZnO nanocomposite with enhanced antimicrobial properties, Int. J. Biol. Macromol. 80 (2015) 121–129.
[10] K.M. Reza, A.S.W. Kurny, F. Gulshan, Parameters affecting the photocatalytic degradation of dyes using TiO2: a review, Appl. Water Sci. 7 (2017) 1569–1578.
[11] U.G. Akpan, B.H. Hameed, Parameters affecting the photocatalytic degradation of dyes using TiO2-based photocatalysts: A review, J. Hazard. Mater. 170 (2009) 520–529.
[12] J.O. Tijani, O.O. Fatoba, G. Madzivire, L.F. Petrik, A Review of Combined Advanced Oxidation Technologies for the Removal of Organic Pollutants from Water, Water Air Soil Poll. 225 (2014) 2102.
[13] L. Zhao, J. Deng, P. Sun, J. Liu, Y. Ji, N. Nakada, Z. Qiao, H. Tanaka, Y. Yang, Nanomaterials for treating emerging contaminants in water by adsorption and photocatalysis: Systematic review and bibliometric analysis, Sci. Total Environ. 627 (2018) 1253–1263.
[14] V. Poza-Nogueiras, E. Rosales, M. Pazos, M.A. Sanromán, Current advances and trends in electro-Fenton process using heterogeneous catalysts – A review, Chemosphere 201 (2018) 399–416.
[15] K. Qi, B. Cheng, J. Yu, W. Ho, Review on the improvement of the photocatalytic and antibacterial activities of ZnO, J. Alloys Compd. 727 (2017) 792–820.
[16] N. Güy, M. Ozacar, The influence of noble metals on photocatalytic activity of ZnO for Congo red degradation, Int. J. Hydrogen Energy 41 (2016) 20100–20112.
[17] V.E. Podasca, T. Buruiana, E.C. Buruiana, UV-cured polymeric films containing ZnO and silver nanoparticles with UV-vis light-assisted photocatalytic activity, Appl. Surf. Sci. 377 (2016) 262–273.
[18] D.W. Gao, Z.D. Wen, Phthalate esters in the environment: a critical review of their occurrence, biodegradation, and removal during wastewater treatment processes, Sci. Total Environ. 541 (2016) 986–1001.
[19] M.Y. Haddad, H.F. Alharbi, M.R. Karim, M.O. Aijaz, N.H. Alharthi, Preparation of TiO2 incorporated polyacrylonitrile electrospun nanofibers for adsorption of heavy metal ions, J. Polym. Res. 25 (2018) 218.
[20] J.S. Im, M. Kim, Y. Lee, Preparation of PAN-based electrospun nanofiber webs containing TiO2 for photocatalytic degradation, Mater. Lett. 62 (2008) 3652–3655.
[21] A. Yar, B. Haspulat, T. Ustun, V. Eskizeybek, A. Avci, H. Kamis, S. Achourd, Electrospun TiO2/ZnO/Pan hybrid nanofiber membranes with efficient photocatalytic activity, RSC Adv. 7 (2017) 29806–29814.
[22] G. Moradi, L. Rajabi, F. Dabirian, S. Zinadini, Biofouling alleviation and flux enhancement of electrospun PAN microfiltration membranes by embedding of para-aminobenzoate alumoxane nanoparticles, J. Appl. Polym. Sci. 135 (2018) 45738.
[23] Y.H. Teow, A.L. Ahmad, J.K. Kim, B.S. Ooi, Studies on the surface properties of mixed-matrix membrane and its antifouling properties for humic acid removal, J. Appl. Polym. Sci. 128 (2013) 3184–3192.
[24] L.Y. Ng, A.W. Mohammed, C.P. Leo, N. Hilal, Polymeric membranes incorporated with metal/metal oxide nanoparticles: A comprehensive review, Desalination 308 (2013) 15–33.
[25] M.K. Arfanis, C.P. Athanasekou, E. Sakellis, N. Boukos, N. Ioannidis, V. Likodimos, L. Sygellou, M. Bouroushian, A.G. Kontos, P. Falaras, Photocatalytic properties of copper—Modified core-shell titania nanocomposites, J. Photochem. Photobiol. A 370 (2019) 145–155.
[26] C.A. Bode-Aluko, O. Pereao, G. Ndayambaje, L. Petrik, Adsorption of Toxic Metals on Modified Polyacrylonitrile Nanofibres: A Review, Water Air Soil Poll. 35 (2017) 228.
[27] C.A. Bode-Aluko, O. Pereao, O. Fatoba, L. Petrik, Surface-modified polyacrylonitrile nanofibres as supports, Polym. Bull. 74 (2017) 2431–2442.
[28] O.K. Pereao, C. Bode-Aluko, G. Ndayambaje, O. Fatoba, L.F. Petrik, Electrospinning: Polymer Nanofibre Adsorbent Applications for Metal Ion Removal, J. Polym. Environ. 25 (2017) 1175–1189.
[29] O.K. Pereao, C. Bode-Aluko, K. Laatikainen, A. Nechaev, L. Petrik, Morphology, Modification and characterisation of electrospun Polymer Nanofiber Adsorbent Material Used in Metal Ion Removal, J. Polym. Environ. 27 (2019) 183–1860.
[30] A. Baji, Y. Mai, S. Wong, M. Abtahi, P. Chen, Electrospinning of polymer nanofibers: Effects on oriented morphology, structures and tensile properties, Compos. sci. Technol. 70 (2010) 703–718.
[31] X. Shi, W. Zhou, D. Ma, Q. Ma, D. Bridges, Y. Ma, A. Hu, Electrospinning of Nanofibers and Their Applications for Energy Devices, J. Nanomater. Vol. 2015, Article ID 140716, 20 pages.
[32] C.A. Bode-Aluko, Functionalisation of polymer nanofibres and track-etched membrane for removal of organic and inorganic pollutants from water, PhD Thesis, University of the Western Cape, Bellville, 2017.
[33] N. Bhardwaj, S. Kindu, Electrospinning: A fascinating fiber fabrication technique, Biotechnol. Adv. 28 (2010) 325–347.
[34] Z. Huang, Y. Zhang, M. Kotaki, S. Ramakrishna, A review on polymer nanofibers by electrospinning and their applications in nanocomposites, Compos. Sci. Technol. 63 (2003) 2223–2253.
[35] S. Nataraj, K. Yang, T. Aminabhavi, Polyacrylonitrile-based nanofibers—A state-of-the-art review, Progr. Polym. Sci. 37 (2012) 487–513.
[36] C.A. Bode-Aluko, K. Laatikainen, O. Pereao, A. Nechaev, I. Kochnev, A. Rossouw, S. Dobretsov, C. Branger, A. Sarbu, L. Petrik, Fabrication and characterisation of novel nanofiltration polymeric membrane, Mat. Today Comm. (2019), 100580.
[37] M. Al-Fori, S. Dobretsov, M.T.Z. Myint, J. Dutta, Antifouling properties of zinc oxide nanorod coatings, Biofouling 30 (2014) 871–882.
[38] J. Zhang, Y. Nosaka, Mechanism of the OH Radical Generation in Photocatalysis with TiO2 of Different Crystalline, Types, J. Phys. Chem. C. 118 (2014) 10824–10832.
[39] H.H. Kyaw, M.T.Z. Myint, S.H. Al-Harthi, T. Maekawa, K. Yanagisawa, A. Sellai, J. Dutta, The influence of initial gold nanoparticles layer on migration of silver nanoparticles in silver/glass matrix, Thin Solid Films 685 (2019) 216–224.
[40] M. Blanco, C. Monteserín, A. Angulo, A. Pérez-Márquez, J. Maudes, N. Murillo, E. Aranzabe, L. Ruiz-Rubio, J. Luis Vilas, TiO2-Doped Electrospun Nanofibrous Membrane for Photocatalytic Water Treatment, Poly. (MDPI) 747 (2019) 11.
[41] A.V. Korobeinyk, R.L. Whitby, S.V. Mikhalovsky, High temperature oxidative resistance of polyacrylonitrile-methylmethacrylate copolymer powder converting to a carbonized monolith, Eur. Polym. J. 48 (2012) 97–104.
[42] J.T. Park, J.H. Koh, J.A. Seo, Y.S. Cho, J.H. kim, Synthesis and characterization of TiO2/Ag/polymer ternary nanoparticles viasurface-initiated atom transfer radical polymerization, Appl. Surf. Sci. 257 (2011) 8301– 8306.

[43] F. He, G. Chen, Y. Yu, S. Hao, Y. Zhou, Y. Zheng, Facile approach to synthesize g-PAN/g- C3N4 composites with enhanced photocatalytic H2 evolution activity, Appl. Mater. Interfaces 6 (2014) 7171–7179.
[44] B. Xing, C. Shi, C. Zhang, G. Yi, L. Chen, H. Guo, G. Huang, J. Cao, Preparation of TiO2/Activated Carbon Composites for Photocatalytic Degradation of RhB under UV Light Irradiation, J. of Nanomater. 10 (2016).
[45] Y. Wang, L. Li, X. Haung, Q. Li, G. Li, New insights into fluorinated TiO2 (brookite, anatase and rutile) nanoparticles as efficient photocatalytic redox catalysts, RSC Adv. 5 (2015) 34302–34313.
[46] S. Tas, O. Kaynan, E. Ozden-Yenigun, K. Nijmeijer, Polyacrylonitrile (PAN)/crown ether composite nanofibers for the selective adsorption of cations, RSC Adv. 6 (2016) 3608–3616.
[47] G.Y. Baek, H.S. Lee, J. Jung, I. Hwang, J. Shin, C. Jung, J. Choi, Preparation of conductive carbon films from polyacrylonitrile/graphene oxide composite films by thermal treatment, J. Ind. Eng. chem. 58 (2018) 87–91.
[48] Y. Zou, J. Shi, D. Ma, Z. Fan, L. Lu, C. Niu, In situ synthesis of C-doped TiO2@g-C3N4 core-shell hollow nanospheres with enhanced visible-light photocatalytic activity for H2 evolution, Chem. Eng. J. 322 (2017) 435–444.
[49] J. Górka, R.T. Mayes, L. Baggetto, G.M. Veith, S. Dai, Sonochemical functionalization of mesoporous carbon for uranium extraction from seawater, J. Mater. Chem. A. 1 (2013) 3016–3026.
[50] C. Yang, B. Wang, Y. Zhang, H. Wang, Preparation and properties of polyacrylonitrile fibers with guanidine groups, Fibers and Polymer A. 16 (2015) 1611–1617.
[51] A. Majumdar, S.C. Das, T. Shripathi, R. Hippler, Chemical synthesis and surface morphology of amorphous hydrogenated carbon nitride film deposited by N2/CH4 dielectric barrier discharge plasma, Compos Interf 19 (2012) 161–170.
[52] X. Bing, W. Xiaoshu, L. Yun, Surface modification of polyacrylonitrile-based carbon fiber and its interaction with imide, Appl. Surf. Sci. 253 (2006) 2695–2701.
[53] L. Pérez-Álvarez, L. Ruiz-Rubio, I. Moreno, J.L. Vilas-Vilela, Characterization and Optimization of the Alkaline Hydrolysis of Polyacrylonitrile Membranes, Polymers 11 (2019) 1843.
[54] H.J. Kwon, C.H. Jung, J.M. Ha, S.O. Cho, J.H. Choi, R. Hippler Shripathi, Synthesis of a Graphene-like Nanofilm from Polyacrylonitrile, J. Nanos. & Nanotechn. 17 (2017) 2503–2507.
[55] K. Trzciński, M. Szkoda, A. Herman, A. Borowska-Centkowska, A. Lisowska-Oleksiak, Does the low optical band gap of yellow Bi3YO6 guarantee the photocatalytical activity under visible light illumination? J. Solid State Electrochem. 22 (2018) 2095–2105.
[56] M.T.Z. Myint, N.S. Kumar, G.L. Hornyak, J. Dutta, Hydrophobic/hydrophilic switching on zinc oxide micro-textured surface, Appl. Surf. Sci. 264 (2013) 344–348.
[57] S. Balu, K. Uma, G.T. Pan, T.C. Yang, S.K. Ramaraj, Degradation of Methylene Blue Dye in the Presence of Visible Light Using SiO2@α-Fe2O3 Nanocomposites Deposited on SnS2 Flowers, Materials 11 (2018) 1030.
[58] H.Q. Nguyen, B. Deng, Electrospinning and in situ nitrogen doping of TiO2/PAN nanofibers with photocatalytic activation in visible lights, Mater. Lett. 82 (2012) 102–104.
[59] B. Al-Ghafri, T. Bora, P. Sathe, S. Dobrestov, M. Al-Abri, Photocatalytic microbial removal and degradation of organic contaminants of water using PES fibers, Appl. Catal. B: Environ. 233 (2018) 136–142.
[60] R.S. Dariani, A.A. Esmaeili, A. Mortezaali, S. Dehghanpour, Photocatalytic reaction and degradation of methylene blue on TiO2 nano-sized particles, Optik 127 (2016) 7143–7154.
[61] R. Zuo, G. Du, W. Zhang, L. Liu, Y. Liu, L. Mei, Z. Li, Photocatalytic Degradation of Methylene Blue Using TiO2 Impregnated Diatomite, Adv. Mater. Sci. Eng. (2014). Article ID 170148.
[62] B. Cabir, M. Yurderi, N. Caner, M.S. Agirtas, M. Zahmakiran, M. Kaya, Methylene blue photocatalytic degradation under visible light irradiation on copper phthalocyanine-sensitized TiO2 nanopowders, Mat. Sci. Eng. B. 224 (2017) 9–17.
[63] K. Norrman, P. Kingshott, B. Kaeselev, A. Ghanbari-Siahkali, Photodegradation of poly (ether sulphone) part 1. A time-of-flight secondary ion mass spectrometry study, Surf. Interface Anal. 36 (2004) 1533-1541.
[64] F. Wang, S. Min, Y. Han, L. Fend, Visible-light-induced photocatalytic degradation of methylene blue with polyaniline-sensitized TiO2 composite photocatalysts, Superlattices Microstruct 48 (2010) 170–180.
[65] M. Zhang, C. Chen, W. Ma, J. Zhao, Visible-light-induced aerobic oxidation of alcohols in a coupled photocatalytic system of dye-sensitized TiO2 and TEMPO, Angew. Chem. Int. Ed. 47 (2008) 9730–9733.
[66] Y. Bessekhouad, N. Chaoui, M. Trzpit, N. Ghazzal, D. Robert, J. Weber, UV–vis Versus Visible Degradation of Acid Orange II in a Coupled CdS/TiO2 Semiconductors Suspension, J. Photochem. Photobiol. A. 183 (2006) 218–224.
[67] L. Yao, X. Song, G. Zhang, S. Xu, Y. Jiang, D. Cheng, Y. Lu, Preparation of Ag/HBP/PAN Nanofiber Web and Its Antimicrobial and Filtration Property, J. Nanomater. (2016). Article ID 4515769.
[68] A. Mahapatra, N. Garg, B.P. Nayak, B.G. Mishra, G. Hota, Studies on the Synthesis of Electrospun PAN-Ag Composite Nanofibers for Antibacterial Application, J. Appl. Polym. Sci. 124 (2012) 1178–1185.
[69] L. Belanger, A. Garenaux, J. Harel, M. Boulianne, E. Nadeau, C.M. Dozois, Escherichia coli from animal reservoirs as a potential source of human extraintestinal pathogenic E. coli, FEMS Immunol. Med. Microbiol. 62 (2011) 1–10.
[70] S.M. Harrington, E.G. Dudley, J.P. Nataro, Pathogenesis of enteroaggregative Escherichia coli infection, FEMS Microbiol. Lett. 254 (2006) 12–18.
[71] T.A. Egerton, S.A.M. Kosa, P.A. Christensen, Photoelectrocatalytic disinfection of E. coli suspensions by iron doped TiO2, Phys. Chem. Chem. Phys. 8 (2006) 398–406.
[72] M. Cho, H. Chung, W. Choi, J. Yoon, Linear correlation between inactivation of E. coli and OH radical concentration in TiO2 photocatalytic disinfection, Water Res. 38 (2004) 1069–1077.
[73] S.H. Hwang, J. Song, Y. Jung, O.Y. Kweon, H. Song, J. Jang, Electrospun ZnO/TiO2 composite nanofibers as a bactericidal agent, Chem. Commun. 47 (2011) 9164–9166.
[74] P. Liu, W. Duan, Q. Wang, X. Li, The damage of outer membrane of Escherichia coli in the presence of TiO2 combined with UV light, Colloids Surf. B. 78 (2010) 171–176.
[75] F.C. Fang, Antimicrobial actions of reactive oxygen species, MBio. 2 (2011) 1–6.
[76] E. Cabiscol, J. Tamarit, J. Ros, Oxidative stress in bacteria and protein damage by reactive oxygen species, Int. Microbiol. 3 (2010) 3–8.
[77] J.A. Imlay, S. Linn, DNA damage and oxygen radical toxicity, Science (Washington) 240 (1988) 1302–1309.